Accepted Manuscript

Flow blurring atomization of Poly(ethylene oxide) solutions below the coil overlap concentration

Miguel Hermosín-Reyes, Alfonso M. Gañán-Calvo, Luis B. Modesto-López

PII: S0021-8502(19)30448-3

DOI: https://doi.org/10.1016/j.jaerosci.2019.105429

Article Number: 105429

Reference: AS 105429

To appear in: *Journal of Aerosol Science*

Received Date: 28 May 2019

Revised Date: 8 July 2019

Accepted Date: 17 July 2019

Please cite this article as: Hermosín-Reyes M, Gañán-Calvo AM, Modesto-López LB, Flow blurring atomization of Poly(ethylene oxide) solutions below the coil overlap concentration, *Journal of Aerosol Science* (2019), doi: https://doi.org/10.1016/j.jaerosci.2019.105429.

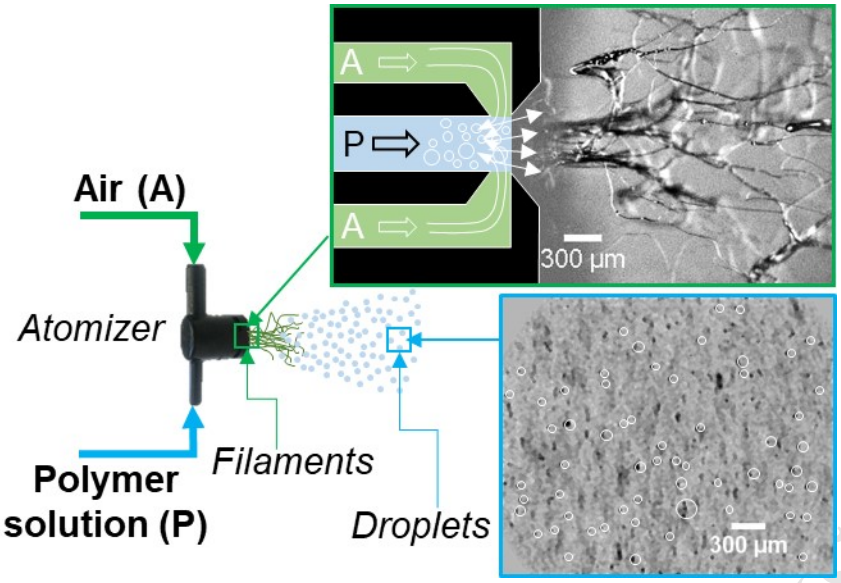

Flow Blurring Atomization of Poly(ethylene oxide) Solutions below the Coil Overlap Concentration

Miguel Hermosín-Reyes, Alfonso M. Gañán-Calvo, Luis B. Modesto-López*

Department of Aerospace Engineering and Fluid Mechanics

University of Seville

Camino de los Descubrimientos S/N, Sevilla 41092, SPAIN

*Corresponding author:

lmodesto@us.es

+34(954) 48-7224

ABSTRACT

Atomization of polymer solutions has important technological implications across many fields. Here, we investigated the atomization dynamics of diluted, polymer solutions using Flow Blurring (FB) technology. Aqueous solutions of poly(ethylene oxide) [PEO] of viscosity-averaged molecular weight in the range 100000 g/mol – 4000000 g/mol and varying concentrations were sprayed with a FB atomizer having an orifice diameter (D) of 700 μm and a liquid feed-tube-to-orifice separation (H) of 100 μm. The solutions belong to the dilute regime, where polymer coil overlap does not occur, that is $\varphi = \frac{c_m M_v}{M_e} < \varphi_{crit}$ (Modesto-López, Pérez-Arjona, & Gañán-Calvo, 2019). Shear viscosity measurements indicated that the solutions had viscosities of the order of that of the solvent and exhibited a Newtonian-like behavior. However, during the atomization, and due to the relatively high shear stress induced in the atomizer, the solutions exhibit extensional rheology, which most likely arises from the stretching of the polymer chains in-flight. Although initially the atomization resulted in formation of filaments, these broke up into droplets at relatively short distances from the atomizer discharge orifice as elucidated by images from ultra-high speed videos. The phenomenon is in contrast with that observed in FB-based atomization of semi-diluted polymer solutions with concentrations larger than the polymer coil overlap concentration, c^*. FB atomization of the diluted solutions resulted in a decrease in droplet size with increasing the gas-to-liquid mass ratio (GLR). The approach herein aims at understanding the droplet formation dynamics of viscoelastic, polymer solutions with FB, for applications in large-scale synthesis of materials.

KEYWORDS: Flow Blurring, Poly(ethylene oxide), Overlap concentration, Droplet size, Extensional Viscosity.

1. INTRODUCTION

Atomization of polymer solutions is of remarkable interest to many technological fields, from agricultural crop spraying, where polymers are added to reduce droplet size and drift, to inkjet printing, where the aim is to avoid formation of satellite droplets that negatively affect the quality of the resulting image (Park & Harrison, 2008; Shore & Harrison, 2005). Processing of materials and powder synthesis are fields where liquid atomization of polymers is highly relevant too. Generally, the polymer's molecular weight and chain conformation influence the physicochemical properties of resulting droplets/particles (Byrappa, Ohara, & Adschiri, 2008; Li, Van Zee, Bates, & Lodge, 2019; Wan et al., 2018). Spraying of polymer solutions together with functional structures, for instance graphene and its derivatives, improves the optical, mechanical, and electrical properties of materials (Liu et al., 2015; Modesto-López, Miettinen, Riikonen, et al., 2015; Modesto-López, Miettinen, Torvela, Lähde, & Jokiniemi, 2015; Schutzius, Bayer, Qin, Waldroup, & Megaridis, 2013). Furthermore, enabling techniques for processing of large quantities of precursors are desirable from an industrial point of view. Thus, understanding the spraying dynamics is paramount to elucidate efficient atomization mechanisms that allow regulation of droplet size and, at some extent, control of the morphology of the sprayed liquid.

Among the wide variety of available spraying techniques, the so-called Flow Blurring (FB) is perhaps the most energetically efficient approach for dispersing bulk liquids into droplets (Gañán-Calvo, 2005; Simmons & Agrawal, 2012). Briefly, the efficacy of the FB mechanism resides in the radial implosion of a gas current into a liquid flow, thus causing a vigorous, turbulent motion in the interior of the liquid, which breaks its surface into droplets (see for instance Figure 3 in Gañán-Calvo (2005)). Similarly, the efficient atomization capabilities of FB devices have been reported by others (Khan, Gadgil, & Kumar, 2019; Niguse & Agrawal, 2015; Rosell-Llompart & Gañán-Calvo, 2008; Simmons & Agrawal, 2010, 2012). Flow Blurring technology has also enabled dispersion of fine water droplets and fuels for combustion-related applications (Niguse & Agrawal, 2015; Serrano et al., 2019; Simmons & Agrawal, 2012).

Recently, we have studied the dynamics of generation of filaments using a FB device from viscous, polymer solutions. The viscosity of aqueous solutions of poly(ethylene oxide) was characterized as a function of a dimensionless parameter, $\varphi = c_m M_v/M_e$. M_v is the polymer's molecular weight, c_m is the concentration in mass fraction, and M_e is the so-called entanglement molecular weight (Heo & Larson, 2005; Tao & Shivkumar, 2007). The zero-shear rate viscosity (η_0) of PEO solutions (see Figure 1a, partially reproduced from Modesto-López et al. (2019)) varies linearly with φ; nevertheless, the slope is different for solutions below and above a critical value of $\varphi = \varphi_{crit}$. Indeed, φ is directly related to the so-called polymer coil overlap concentration c^*, which delimits the transition from a dilute to a semi-concentrated solution. Thus, $\varphi_{crit} = c^* M_v/M_e$ sets the onset for filament production with FB. For PEO solutions with $\varphi > \varphi_{crit}$, η_0 scales as $\varphi^{3.2}$ and in this regime the atomization produces filamentous/fibrous structures (Modesto-López et al., 2019). Here, however, we delve into the dynamics of the FB-atomization of diluted, aqueous PEO solutions, in the region where $\varphi < \varphi_{crit}$. There, η_0 scales as φ and polymer coil overlap is not expected to occur, yet intriguing phenomena associated to the liquid's rheology are observed (Clasen, Phillips, Palangetic, & Vermant, 2012; Colby, Boris, Krause, & Dou, 2007; Larson, 2005).

2. EXPERIMENTAL SECTION

2.1 Materials

Poly(ethylene oxide) [PEO] of viscosity-averaged molecular weight, M_v, 100000 g/mol (100k), 600000 g/mol (600k), 1000000 g/mol (1M), 2000000 g/mol (2M), and 4000000 g/mol (4M) were purchased from Sigma-Aldrich and used as received. Distilled water (Milli Q) was used as solvent. For atomization experiments, the FB device has an orifice diameter (D) of 700 μm and a liquid feed tube-to-orifice distance (H) of 100 μm, resulting in a $\phi = H/D$ of 1/7 (see Figure 1b).

2.2 Solution Preparation, Viscosity and Surface Tension Measurements

Polymeric solutions of different concentrations were prepared by adding an appropriate amount of PEO to distilled water, followed by mixing with a magnetic stirrer until a uniform solution was obtained. Typical stirring times were of the order of one day, in some cases, mild heating was applied to facilitate mixing, particularly in the case of PEO of higher molecular weight and relative high concentration. The solutions were cooled at room temperature prior to use. Subsequently, the viscosity was measured using a Brookfield DV-E instrument equipped with LV type spindles, in the shear rate range of 1 s^{-1} - 100 s^{-1}. All measurements were performed at room temperature (19 ℃ - 24 ℃) and ambient relative humidity (40 % - 60 %). Solutions were allowed to stabilize for a few minutes before recording any measurement.

The surface tension of polymeric solutions in air was measured with a KSV contact angle meter (CAM 100) set up in a pendant drop configuration, for static measurements in the range 0° - 180°. The instrument is equipped with a FireWire video camera module with a resolution of 640 x 480 pixels and with a LED, monochromatic, light source. The objective lens provided with the camera is telecentric with a 55-mm focus length. The instrument's software applies a curve fitting using the Young-Laplace equation to calculate surface tension.

2.3 Flow Blurring Atomization, Size Measurement with Light Scattering and High-speed Video Recording

The FB atomization system has been described in a previous publication, see Modesto-López *et al.* (2019) for details. Briefly, the atomizer was mounted on an optical table using high-precision, movable mounts, which allowed to displace it forward and backward along a straight center line. Here, z is the distance from the atomizer outlet. The atomizer was operated by controlling the pressures of gas, air in this case, and liquid supply lines. The air was fed into the FB atomizer directly from the supply line while the liquid was fed pneumatically through a hermetic liquid container. A check valve was placed between the liquid container and the atomizer inlet to avoid back flow. Both, gas and liquid pressures were measured by digital manometers. The FB atomizer was operated by first fixing the air pressure (P_G) in the range 100 kPa - 300 kPa, and then adjusting the liquid pressure (P_L) until a continuous, stable atomization was achieved. A calibration curve of liquid flow rate, Q_ℓ, as a function of liquid pressure was established for each gas pressure used in the experiments. Q_ℓ was obtained by measuring the volume of polymer solutions coming out the FB device for a given period of time. Figure 2 depicts the evolution of Q_ℓ as a function of $\Delta P_L = P_L - P_G^*$, where $P_G^* = P_G - P_o$ and P_o is the atmospheric pressure. Typical liquid flow rates used in this work are thus in the range 0.35 – 1.50 mL/s.

Videos of the atomization process were recorded at varying z using a Shimadzu ultra-high-speed HPV-2 video camera capable of recording up to 10^6 frames per second (fps) at a 312 x 260-pixel resolution. The videos were illuminated with a high-intensity Walimex Pro Studio Flash (VC-4000) positioned on the opposite side of the camera, across the FB atomizer. The flash was synchronized with the video camera's power unit through an external trigger. The camera was focused along the centerline of the

atomization output and began recording 1 ms after the trigger was manually switched on. The videos were processed with ImageJ, a freeware image processing software, to remove their background (static objects), optical artifacts, and noise.

Droplet size distribution were obtained with a Malvern Spraytec® system equipped with a 632.8-nm He-Ne laser of 15 mm in diameter and with a 300-mm range lens system capable of measuring particles with size in the range 0.1 – 900 μm. The detection system consists of 36 elements log-spaced silicon diode array. It has a maximum acquisition rate of 2.5 kHz (Rapid mode). Size distribution measurements were recorded at a distance from the atomizer outlet of $z = 4\ cm$. To further gain insights into the nature of the size distributions, they were fitted with log-normal profiles using a commercial software (Igor Pro v. 6.37).

3. RESULTS AND DISCUSSION

In general, polymer solutions exhibit a complex rheology associated mainly to their molecular weight and their concentration (Bouldin, Kulicke, & Kehler, 1988; Clasen et al., 2006; Colby et al., 2007). In our previous study of FB-enabled atomization of polymer solutions, we determined that there exists a φ_{crit} directly related to the polymer coil overlap concentration, c^*, above which only filaments are ejected from the atomizer (see Figure 3 in Modesto-López *et al.* (2019)). Once out of the device, these structures do not undergo subsequent breakup, but instead maintain their filamentous shape even at relatively large z. However, in the region $\varphi < \varphi_{crit}$ polymer chains do not overlap and our preliminary experiments indicate that droplets instead of filaments are produced at $z \geq 4\ cm$. These regimes appear to be independent of the FB process parameters, that is, liquid flow rate and gas pressure (Modesto-López et al., 2019). Dilute polymer solutions with concentration below c^*exhibit a zero-shear rate viscosity of the order of the solvent viscosity as shown in Figure 1a (partially reproduced from Modesto-López *et. al.* (2019)). Despite their low concentration and thus low η_0, several authors have reported that these solutions exhibit a viscoelastic nature and display extensional viscosity, and therefore a complex rheological behavior. It is thus important to first address the viscous properties of these solutions.

3.1 Viscosity of PEO aqueous solutions

Figure 1c depicts the viscosity of PEO solutions investigated in this study as a function of shear rate. In the measured range, the solutions appear to be Newtonian, with viscosity values of the order of that of the solvent (1 $mPa \cdot s$). Our results agree with data reported elsewhere and measured with a variety of different instruments (Ebagninin, Benchabane, & Bekkour, 2009; Giudice et al., 2014; Mun, Young, & Boger, 1999; Shore & Harrison, 2005; Sousa, Vega, Sousa, Montanero, & Alves, 2017). For instance, Park and Harrrison (2008) measured the viscosity of 100k-PEO 0.6 $wt\%$ and 600k-PEO 0.05 $wt\%$ to be 4.41 cP and 4.69 cP, respectively. Such values were of the order of that of the pure solvent, a glycerol/water mixture (50/50 $wt\%$) of 4.58 cP. Sousa *et al.* (2017) reported a viscosity for a 1M-PEO of 0.05 $wt\%$ to be $\sim$ 6 cP in a glycerol/water mixture (40/60 $wt\%$). Tirel and co-workers (2017) measured the viscosity of a 8M-PEO 0.0005 $wt\%$ to be 1.34 cP in an isopropyl alcohol/water mixture (5/95 $wt\%$). Furthermore, Tirtaatmadja and coauthors (2006) reported the viscosities of 600k-PEO 0.17 $wt\%$, 1M-PEO 0.1 $wt\%$, and 2M-PEO 0.05 $wt\%$ in glycerol/water mixtures to be 5.9 cP, 5.8 cP, and 5 cP, respectively. Those studies emphasize the highly viscoelastic nature of PEO solutions even at very low concentration (Park & Harrison, 2008; Sousa et al., 2017; Tirel et al., 2017; Tirtaatmadja et al., 2006). Next, to investigate the dynamics of atomization of aqueous solutions with FB, high-speed

videos were recorded to capture the early stages of the process. Furthermore, although not investigated herein, it is important to highlight that the viscoelasticity of PEO aqueous solutions is influenced by the polymer molecular weight distribution. Kulicke *et al*. report that aqueous solutions prepared with commercially obtained PEO of a wide molecular weight distribution exhibited a marked non-Newtonian behavior compared to PEO of narrow molecular weight distribution, which showed a nearly Newtonian profile (Kulicke, Elsabee, Eisenbach, & Peuscher, 1983).

3.2 Ejection of filaments and formation of droplets

Ultra-high-speed videos of FB-atomized solutions with different zero-shear rate viscosities of 4.75 cP (100k, 2.0 wt%) and 1.71 cP (600k, 0.1 wt%) were recorded at $z = 0\ cm$, the atomizer's outlet, and at z= 4 cm. The pressures employed for these experiments were $P_G = 100\ kPa$ and $P_L \sim 78\ kPa$, which resulted in liquid flow rates of $Q_\ell = 0.375\ mL/s$ and $Q_\ell = 0.536\ mL/s$ for the 4.75-cP and 1.71-cP solutions, respectively. Figure 3a shows an image of the FB atomization of the solution with the highest η_0 at $z = 0\ cm$, and Figure 3b shows an image of that at $z = 4\ cm$, note that the images belong to different atomization events under similar experimental conditions. Initially, filaments with varying diameters of the order of $100\ \mu m$ come out of the atomizer. During the atomization of water with FB devices Gañán-Calvo (2005) and Rosell-Llompart and Gañán-Calvo (2008) observed ligaments right at the atomizer outlet. The formation of those depends on the so-called capillary time, which in case of water, a Newtonian fluid, is of the order of microseconds. It is important to note that in the work of Gañán-Calvo (2005) and Rosell-Llompart and Gañán-Calvo (2008) the devices' orifice had diameters between three and ten times larger than the one used in this study. Using an ultra-high speed video camera Modesto-López and Gañán-Calvo (2018) observed that during a FB-based atomization of water in pressurized environments droplets, instead of filaments, come out the atomization device. However, in our experiments at $z = 4\ cm$, conversely to $z = 0\ cm$ the filaments are no longer observed, instead they have broken into droplets despite the relatively large viscosity of the solution. In the case of the atomization of the solution with η_0= 1.71 cP, in addition to the filaments, droplets come out the device (Figure 3c). These filaments appear to be thinner than those in Figure 3a. In this case too, a significantly large fraction of the filaments have been transformed into droplets at $z = 4\ cm$ as shown in the image of Figure 3d. Nevertheless, there are some atomization events of the 1.71-cP solution where relatively short, thin filaments are present even at $z = 4\ cm$, as depicted in Figures 3e and 3f. While in Figure 3e the filament appears linking two droplets (see red oval in the figure) in Figure 3f they emanate from a single droplet forming a "tail". The mechanism of formation of these short filaments remains unknown, however, their presence can be most probably attributed to the viscoelastic nature of the solutions, which undergo extensional rheology and stretch out due to the tangential stresses exerted by the acceleration as they move forward. Next, images of the early stages of the atomization of the 1.71-cP solution (PEO 600k, 0.1 $wt\%$, $P_G = 100\ kPa$, $Q_\ell = 0.536\ mL/s$) are discussed in more detail. Figure 4 shows sequential images of the atomization recorded in the region close to the atomizer outlet; the time between each frame being 1 μs. The images depict several filaments breaking up into droplets at a very high rate. For instance, the red oval highlights a bulk of solution structure that extends its overall dimensions simultaneously thinning the diameter of the filaments that form it. In frame 1, the characteristic length of the "chunk" enclosed in the oval is roughly $600\ \mu m$ while 20 μs later (frame 20) and just $\sim 600\ \mu m$ farther in the axial direction, it has doubled its length. In other words, in the region close to the atomizer's outlet the filaments stretch at a rate of roughly $30\ m/s$. Note that as the camera is focused on the central plane of the atomization and perpendicularly to the axial direction of the motion of the gas and liquid flows. It thus records the motion of filament in one direction only, that is, the axial direction. Therefore, while stretching of filaments may be occurring simultaneously in other directions the camera does not capture such

movements. As a consequence, the elongation rates reported herein correspond to those observed along the axial direction. Interestingly, the filament below the oval, pointed out by a white, dashed line in some frames, does not appear to significantly reduce its characteristic diameter but only follows an undulating motion as it travels downstream, as if the polymer chains in the filament were expanded already. This points to the fact that the ligaments located at the periphery of the two-phase jet near the exit of the nebulizer undergo significantly smaller strain rates due to the presence of smaller turbulent stresses. Similarly to our results, Park and Harrison observed the formation of droplets linked by thin filaments during the spraying of PEO solutions using a Turbo Tee Jet nozzle (Park & Harrison, 2008). However, the droplets produced by them had a relatively large mean size, of the order of 1 mm. Park and Harrison attributed the filament formation to the extensional rheology of the solutions. In their work, the number of filaments increased with rising the polymer molecular weight as well as the solution's concentration, that is, increasing the viscoelastic nature of the atomizing solution. Furthermore, in the work of Park and Harrison (2008), solutions with molecular weight larger than 300k (0.5 $wt\%$) formed filaments at distances as far as $z = 13\ cm$, and their presence decreased significantly at $z = 17\ cm$. In contrast, in our experiments, both the length scales and the diameters of filaments and droplets are much smaller, with filaments disappearing at distances as close as $z = 4\ cm$. This shorter length scales most likely result from an efficient mixing due to the turbulent motion in the interior of the FB atomizer.

Ancillary experiments demonstrate the viscoelastic nature of these dilute solutions. During the atomization of a 100k PEO solution of 1.5 wt% ($P_G = 200\ kPa, Q_\ell = 0.54\ mL/s$) we were able to capture the in-flight collision of two droplets as depicted in the sequential images of Figure 5. A ~ 60-μm droplet accelerates and impacts a ~ 40-μm droplet. They do not coalesce, but instead a thin filament is formed between the two as the larger droplet passes through the smaller one. As they continue their motion, the filament elongates, thus reducing the size of the 40-μm droplet. These phenomena are significantly different from the case when two droplets of a Newtonian fluid collide (Finotello et al., 2018; Qian & Law, 1997; Shao, Luo, Chai, & Fan, 2018); in such case no filament is formed but instead a small satellite droplet is ejected during the collision. In frame 6, an initial diameter of the filament can be established as $D_0 = 2R_0$. Figure 5b shows the evolution of the filament's dimensionless radius $R^* = R/R_0$ as a function of a characteristic dimensionless time, τ^*, which was calculated by non-dimensionalizing the time of the process, t, with a characteristic capillary time, $t_c = \left(\frac{\rho R^3}{\sigma}\right)^{1/2}$, where R is the filament radius at each frame, ρ and σ are the density and surface tension of the polymer solution, respectively. The plot clearly shows two distinct regimes, with a transition at $\tau^* \sim \mathcal{O}(1)$. For $\tau^* < 1$, R^*decreases as $-0.773{\tau^*}^{0.44}$ and for τ^* larger than unity R^* scales as ~ 0.227. The evolution of the filament is in good agreement with inertia-capillary and elasto-capillary phenomena of filaments of viscoelastic solutions and usually reported in rheological studies (Anna & McKinley, 2001; Mckinley, 2005; Tirel et al., 2017). In the so-called inertio-capillary regime, the filament radius decreases linearly with time, up to a point where elastic forces become relevant and the elasto-capillary regime takes over (Anna & McKinley, 2001; Dinic, Zhang, Jimenez, & Sharma, 2015; Mckinley, 2005). From the plot, the droplet characteristic pinching time is thus estimated to be $\sim 4.12\ \mu s$. In Newtonian solutions the approach to the pinch point, which in such fluids corresponds to the point of rupture, is extremely rapid encompassing a sudden increase in curvature, thus producing very large extension rates at this location that may cause breakup of the necked fluid. However, in viscoelastic, polymer solutions their molecules are significantly extended, causing a localized increase in the elastic stresses, which grow to balance the capillary pressure, thus preventing the necked fluid from breaking off. Alternatively, a cylindrical filament forms in which elastic stresses and capillary pressure balance each other, and the radius decreases exponentially with time (Tirtaatmadja et al., 2006). Although theoretically an estimation of the relaxation time, λ, can be obtained by an exponential

fitting of the data in the elasto-capillary regime with $R/R_o = Aexp\left\{-\frac{t}{3\lambda}\right\}$, the lack of sufficient data points does not allow us to obtain a reasonable value. Nevertheless, the transition from the inertio-capillary to the elasto-capillary regimes is clearly appreciated both from the video frames and from the plot, thus demonstrating the viscoelastic nature of this diluted solution.

3.3 Droplet size as a function of gas-to-liquid mass ratio

The droplet size was studied as a function of the process parameters such as the gas pressure and the gas-to-liquid mass ratio (GLR), which is typically used to assess the size of droplets produced during an atomization process. The droplet size distributions of all polymer solutions were measured at P_G of 100 kPa, 200 kPa, and 300 kPa and varying liquid flow rates. Figure 6 shows a typical droplet size distribution of solutions sprayed with FB; in this particular case, the distributions correspond to PEO of 100k and 1.5 $wt\%$ at $P_G = 300\ kPa$, and varying Q_ℓ of 1.09 mL/s, 1.33 mL/s, and 1.42 mL/s. The plots show an initially broad distribution, ranging from 0.1 μm to $\sim$ 200 μm, at the lowest liquid flow rate with a small shoulder at $\sim$ 400 μm. The mean droplet diameter shifts towards a larger size with increasing Q_ℓ simultaneously decreasing the fraction of small droplets. The measurements appear to be very sensitive to Q_ℓ, the figure shows that a rise of $\sim$ 22 % in Q_ℓ causes a shift of the main peak from $\sim$ 10 μm to 40 μm, and subsequently to $\sim$ 70 μm with a further increment of $\sim$ 7 % of Q_ℓ, while the position of the shoulder at 400 μm remained nearly constant. Inspection of the size distributions evidence that the main broad line is formed by the superposition of at least two log-normal lines. All measured distributions were fitted with lognormal functions and their dimensionless, mean diameters, d_1^* and d_2^* are plotted in Figure 7. Here, $d_1^* = d_1/D$ and $d_2^* = d_2/D$, where D is the diameter of the orifice of the FB atomizer and d_1 and d_2 are the mean diameters of the two main lines obtained from the lognormal fitting. d_1^* scales as $d_2^{*1.64}$ and interestingly, as the dimensionless diameters grow they approach the orifice mean diameter, D. An increase of either d_1^* or d_2^* is caused by an increase of the liquid flow rate, thus implying that at a sufficiently high Q_ℓ the produced droplets are of the order of the FB atomizer's orifice diameter.

Figure 8 shows the mean diameter d_2 made non-dimensional with the minimum attainable diameter D_o, that is $d^+ = d_2/D_o$, as a function of the gas-to-liquid mass ratio (GLR). $D_o = \sigma/\Delta P$ and ΔP is the gas pressure drop across the FB device (Rosell-Llompart & Gañán-Calvo, 2008). The *GLR* is associated to the energy supplied to the bulk liquid to break it into small droplets by the turbulent motion. Therefore, increasing the *GLR* implies that the kinetic energy transported by the gas current is increased, thus enhancing the production of smaller droplets compared to lower *GLR*s. This trend is evidenced by the plot of Figure 8, in which a power law fit results in the following scaling parameter: $d^+ = 0.816GLR^{-2.49}$, and it depicts data points corresponding to each gas pressure. In general, a higher gas pressure results in larger values of the dimensionless mean diameter d^+. For $GLRs < 0.1$, the d_2 is at least two orders of magnitude larger than D_o; conversely, for $GLRs > 0.1$, d_2 tends towards smaller values, and perhaps approaching D_o. Broniarz and coauthors sprayed diluted PEO solutions, with viscosities in the range of the ones used in this study, using an effervescent atomizer, which functions with a different mechanism. Although the sizes they report are of the order of a few millimeters, the tendency is similar to our data, that is, the droplet size decreases with increasing the *GLR* (Broniarz-Press, Ochowiak, & Woziwodzki, 2010).

To study the atomization characteristics of the FB device with these solutions, the flow discharge coefficient (C_D), which represents the ratio of measured mass flow rate to theoretical mass flow rate for our FB atomizer, was calculated with $C_D = Q_{m,\ell}/A_o(2\rho\Delta P_L)^{1/2}$,where $Q_{m,\ell}$ is the solution mass flow rate, A_o is the cross-sectional area of the atomizer discharge orifice, ρ is the density of the solution, and

ΔP_L is the liquid pressure drop across the atomizer. Figure 9 depicts C_D as a function of the gas-to-liquid mass ratio (GLR). Naturally, the data indicate that for a given GLR rising the gas pressure results in a decrease of the discharge coefficient, thus reducing the actual mass of atomized solution. Higher values of GLR imply an enhancement of the turbulence in the atomizer's interior, thus increasing the hydraulic resistance, that is $\frac{\Delta P_L}{Q_\ell}$. It is also interesting to point out that for a given P_G value, all data points collapse into a single line independently of the zero-shear rate viscosity of the solution, which was different for each of them. Fitting of the C_D data as function of GLR gives the following relations $C_{D_1} = 0.0172GLR^{-0.944}$, $C_{D_2} = 0.0124GLR^{-0.927}$, and $C_{D_3} = 0.0103GLR^{-0.914}$ for $P_G = 100, 200,$ and 300 kPa, respectively.

Figure 10 shows the Reynolds (Re) and Deborah (De) numbers as a function of GLR. Re was calculated as $\rho_m v_m D/\eta_0$, where ρ_m and v_m are the air-solution mixture's density and velocity obtained using the volume fraction of air and the polymer solution, since they both simultaneously leave the atomizer's orifice (Khan et al., 2019). De is the ratio of a time of relaxation (λ) to a characteristic time of the process (θ). The Rouse-Zimm model was used to calculate the relaxation time of the polymer solutions with $\lambda_z \cong \frac{1}{\zeta(3\nu)}\frac{[\eta]M_v\eta_s}{N_A k_B T}$, where the intrinsic viscosity with units of mL/g was obtained with $[\eta] = 0.0125M_v^{0.78}$ for PEO in water, η_s is the solvent viscosity, N_A is Avogadro's number, k_B is the Boltzmann constant, and T is the absolute temperature. In the limit of dominant hydrodynamic interactions the function $\frac{1}{\zeta(3\nu)}$ takes the value of 0.422 (Dinic, Biagioli, & Sharma, 2017; Greiciunas et al., 2017; Tirtaatmadja et al., 2006). The characteristic time of the FB atomization process θ was calculated with $\frac{\pi D^2 H}{4Q_\ell}$. Figure 10a shows a tendency of the Reynolds number to decrease as the GLR increases, indeed Re decreases nearly two-fold as the GLR varies from ~ 0.06 to ~ 0.3. These results evidence the important role of viscosity during FB in addition to the geometrical criterion established by Gañán-Calvo (2005). Furthermore, for a given GLR, polymer solutions with larger η_0 exhibit lower Re most likely because the increased dominance of viscous mechanisms dampen inertial effects. The lines in the plot are exponential fittings to guide the eye. In Figure 10b the Deborah number for each PEO molecular weight is plotted as a function of GLR. Solutions of PEO of higher molecular weight show larger De, thus implying their relaxation time is significantly larger than PEO of lower molecular weight. Indeed, increasing M_v one order of magnitude from 100k to 1M causes an increase in De of a similar order. Additionally, for a given molecular weight the Deborah number decreases as the GLR is increased, which means that the augment in energy associated with the FB mechanism improves the solutions' capability the flow and the relaxation time scale is reduced in comparison with the time scale of the atomization. These results correlate well with those of Figure 8, where a smaller d^+ is obtained with larger GLRs.

4. CONCLUSION

PEO solutions of varying molecular weights and concentrations below the polymer' coil overlap concentration c^*were atomized using the Flow Blurring mechanism. Although, viscosity measurements show the nearly Newtonian behavior of these fluids, images from high-speed videos of the atomization process show that in flight these solutions exhibit viscoelastic nature, even those of PEO of the lowest $M_v = 100k$. Although at very early stages of the atomization procedure filaments form, they evolve into droplets in a relatively short distance from the atomizer outlet; and at $z = 4\ cm$ a cloud of droplets is already observed. Droplet size measurements using light-scattering equipment indicate a broad distribution for all solutions and FB conditions. Nevertheless, careful inspection of their plots reveal

that they arise from the contribution of two main lognormal profiles, and their mean diameters exhibit a linear dependence. Furthermore, the general tendency shows that rising the GLR causes a reduction of the dimensionless diameter of the second peak. Higher liquid pressures result in smaller GLRs and thus larger droplet size for a relatively narrow range of GLR. That is, at smaller GLR, the sensitivity of the mean droplet size is higher than that of larger values of GLR. The Reynolds number, based on the density and velocity of the air-solution mixture coming out the atomizer, as a function of GLR, shows a characteristic line for each of the solutions used in this work. Furthermore, the ability of PEO solutions to flow augments with increasing the GLR. This study sheds light into the breakup dynamics of Flow Blurring-based atomization of polymer solutions.

5. ACKNOWLEDGEMENTS

A.M.G.-C. and L.B.M.-L. acknowledge financial support from the Ministerio de Economía y Competitividad del Gobierno de España, through the Plan Estatal program (grant DPI2016-78887-C3-1-R.)

6. REFERENCES

Anna, S. L., & McKinley, G. H. (2001). Elasto-capillary thinning and breakup of model elastic liquids. *Journal of Rheology*. https://doi.org/10.1122/1.1332389

Bouldin, M., Kulicke, W. M., & Kehler, H. (1988). Prediction of the non-Newtonian viscosity and shear stability of polymer solutions. *Colloid & Polymer Science*, *266*(9), 793–805. https://doi.org/10.1007/BF01417863

Broniarz-Press, L., Ochowiak, M., & Woziwodzki, S. (2010). Atomization of PEO aqueous solutions in effervescent atomizers. *International Journal of Heat and Fluid Flow*, *31*(4), 651–658. https://doi.org/10.1016/j.ijheatfluidflow.2010.02.005

Byrappa, K., Ohara, S., & Adschiri, T. (2008). Nanoparticles synthesis using supercritical fluid technology – towards biomedical applications. *Advanced Drug Delivery Reviews*, *60*(3), 299–327. https://doi.org/10.1016/J.ADDR.2007.09.001

Clasen, C., Phillips, P. M., Palangetic, L., & Vermant, J. (2012). Dispensing of rheologically complex fluids: The map of misery. *AIChE Journal*, *58*(10), 3242–3255. https://doi.org/10.1002/aic.13704

Clasen, C., Plog, J. P., Kulicke, W.-M., Owens, M., Macosko, C., Scriven, L. E., … McKinley, G. H. (2006). How dilute are dilute solutions in extensional flows? *Journal of Rheology*, *50*(6), 849–881. https://doi.org/10.1122/1.2357595

Colby, R. H., Boris, D. C., Krause, W. E., & Dou, S. (2007). Shear thinning of unentangled flexible polymer liquids. *Rheologica Acta*, *46*(5), 569–575. https://doi.org/10.1007/s00397-006-0142-y

Dinic, J., Biagioli, M., & Sharma, V. (2017). Pinch-off dynamics and extensional relaxation times of intrinsically semi-dilute polymer solutions characterized by dripping-onto-substrate rheometry. *Journal of Polymer Science Part B: Polymer Physics*, *55*(22), 1692–1704. https://doi.org/10.1002/polb.24388

Dinic, J., Zhang, Y., Jimenez, L. N., & Sharma, V. (2015). Extensional Relaxation Times of Dilute, Aqueous Polymer Solutions. *ACS Macro Letters*, *4*(7), 804–808.

https://doi.org/10.1021/acsmacrolett.5b00393

Ebagninin, K. W., Benchabane, A., & Bekkour, K. (2009). Rheological characterization of poly(ethylene oxide) solutions of different molecular weights. *Journal of Colloid and Interface Science*, *336*(1), 360–367. https://doi.org/10.1016/j.jcis.2009.03.014

Finotello, G., Roeland, ·, Kooiman, F., Padding, J. T., Buist, K. A., Jongsma, · Alfred, … Kuipers, J. A. M. (2018). The dynamics of milk droplet-droplet collisions. *Experiments in Fluids*, *59*, 17. https://doi.org/10.1007/s00348-017-2471-2

Gañán-Calvo, A. M. (2005). Enhanced liquid atomization: From flow-focusing to flow-blurring. *Applied Physics Letters*, *86*(21), 1–3. https://doi.org/10.1063/1.1931057

Giudice, F. Del, D'avino, G., Greco, F., De Santo, I., Ab, P. A. N., Luca, P., & Ab, M. (2014). Lab on a Chip Rheometry-on-a-chip: measuring the relaxation time of a viscoelastic liquid through particle migration in microchannel flows. *Lab on a Chip*, *15*, 783–792. https://doi.org/10.1039/c4lc01157k

Greiciunas, E., Wong, J., Gorbatenko, I., Hall, J., Wilson, M. C. T., Kapur, N., … Threlfall-Holmes, P. (2017). Design and operation of a Rayleigh Ohnesorge Jetting Extensional Rheometer (ROJER) to study extensional properties of low viscosity polymer solutions. *Journal of Rheology*, *61*(3), 467–476. https://doi.org/10.1122/1.4979099

Heo, Y., & Larson, R. G. (2005). The scaling of zero-shear viscosities of semidilute polymer solutions with concentration. *Journal of Rheology*, *49*(5), 1117–1128. https://doi.org/10.1122/1.1993595

Khan, M. A., Gadgil, H., & Kumar, S. (2019). Influence of liquid properties on atomization characteristics of flow-blurring injector at ultra-low flow rates. *Energy*, *171*, 1–13. https://doi.org/10.1016/J.ENERGY.2019.01.006

Kulicke, W.-M., Elsabee, M., Eisenbach, C. D., & Peuscher, M. (1983). Effect of molecular weight and molecular weight distribution on the rheological properties of aqueous poly(ethylene oxide) solution. *Polymer Bulletin*, *9*, 190–197. https://doi.org/10.1007/BF00283706

Larson, R. G. (2005). The rheology of dilute solutions of flexible polymers: Progress and problems. *Journal of Rheology*, *49*(1), 1–70. https://doi.org/10.1122/1.1835336

Li, Z., Van Zee, N. J., Bates, F. S., & Lodge, T. P. (2019). Polymer Nanogels as Reservoirs To Inhibit Hydrophobic Drug Crystallization. *ACS Nano*, *13*, 1232–1243. https://doi.org/10.1021/acsnano.8b06393

Liu, Z., Parvez, K., Li, R., Dong, R., Feng, X., & Müllen, K. (2015). Transparent Conductive Electrodes from Graphene/PEDOT:PSS Hybrid Inks for Ultrathin Organic Photodetectors. *Advanced Materials*, *27*(4), 669–675. https://doi.org/10.1002/adma.201403826

Mckinley, G. H. (2005). Visco-elasto-capillary thinning and break-up of complex fluids. In D. M. . Binding & K. Walters (Eds.), *Rheology Reviews* (pp. 1–49). Aberystwyth, U.K: British Society of Rheology. Retrieved from http://www.bsr.org.uk

Modesto-López, L. B., & Gañán-Calvo, A. M. (2018). Visualization and size-measurement of droplets generated by Flow Blurring® in a high-pressure environment. *Aerosol Science and Technology*, *52*(2), 198–208. https://doi.org/10.1080/02786826.2017.1390207

Modesto-López, L. B., Miettinen, M., Riikonen, J., Torvela, T., Pfüller, C., Lehto, V.-P., … Jokiniemi, J. (2015). Films of graphene nanomaterials formed by ultrasonic spraying of their stable suspensions. *Aerosol Science and Technology*, *49*(1), 45–56.

https://doi.org/10.1080/02786826.2014.991438

Modesto-López, L. B., Miettinen, M., Torvela, T., Lähde, A., & Jokiniemi, J. (2015). Direct deposition of graphene nanomaterial films on polymer-coated glass by ultrasonic spraying. *Thin Solid Films*, *578*, 45–52. https://doi.org/10.1016/j.tsf.2015.01.073

Modesto-López, L. B., Pérez-Arjona, A., & Gañán-Calvo, A. M. (2019). Flow Blurring-Enabled Production of Polymer Filaments from Poly(ethylene oxide) Solutions. *ACS Omega*, *4*(2), 2693–2701. https://doi.org/10.1021/acsomega.8b02542

Mun, R. P., Young, B. W., & Boger, D. V. (1999). Atomisation of dilute polymer solutions in agricultural spray nozzles. *Journal of Non-Newtonian Fluid Mechanics*, *83*(1–2), 163–178. https://doi.org/10.1016/S0377-0257(98)00135-9

Niguse, Y., & Agrawal, A. (2015). Low-Emission, Liquid Fuel Combustion System for Conventional and Alternative Fuels Developed by the Scaling Analysis. *Journal of Engineering for Gas Turbines and Power*, *138*(4), 041502. https://doi.org/10.1115/1.4031475

Park, G. Y., & Harrison, G. M. (2008). Effects of elasticity on the spraying of a non-Newtonian fluid. *Atomization and Sprays*, *18*(3), 243–271. https://doi.org/10.1615/AtomizSpr.v18.i3.20

Qian, J., & Law, C. K. (1997). Regimes of coalescence and separation in droplet collision. *J. Fluid Mech*, *331*, 59–80. https://doi.org/10.1017/S0022112096003722

Rosell-Llompart, J., & Gañán-Calvo, A. M. (2008). Turbulence in pneumatic flow focusing and flow blurring regimes. *Physical Review E - Statistical, Nonlinear, and Soft Matter Physics*, *77*(3), 1–10. https://doi.org/10.1103/PhysRevE.77.036321

Schutzius, T. M., Bayer, I. S., Qin, J., Waldroup, D., & Megaridis, C. M. (2013). Water-Based, Nonfluorinated Dispersions for Environmentally Benign, Large-Area, Superhydrophobic Coatings. *ACS Applied Materials & Interfaces*, *5*, 13419–13425. https://doi.org/10.1021/am4043307

Serrano, J., Jiménez-Espadafor, F. J., Lora, A., Modesto-López, L., Gañán-Calvo, A., & López-Serrano, J. (2019). Experimental analysis of NOx reduction through water addition and comparison with exhaust gas recycling. *Energy*, *168*, 737–752. https://doi.org/10.1016/J.ENERGY.2018.11.136

Shao, C., Luo, K., Chai, M., & Fan, J. (2018). Sheet, ligament and droplet formation in swirling primary atomization. *AIP Advances*, *8*, 45211. https://doi.org/10.1063/1.5017162

Shore, H. J., & Harrison, G. M. (2005). The effect of added polymers on the formation of drops ejected from a nozzle. *Phys. Fluids*, *17*, 33104. https://doi.org/10.1063/1.1850431

Simmons, B. M., & Agrawal, A. K. (2010). Spray characteristics of a Flow-Blurring atomizer. *Atomization and Sprays*, *20*(9), 821–835. https://doi.org/10.1615/AtomizSpr.v20.i9.60

Simmons, B. M., & Agrawal, A. K. (2012). Flow blurring atomization for low-emission combustion of liquid biofuels. *Combustion Science and Technology*, *184*(5), 660–675. https://doi.org/10.1080/00102202.2012.660222

Sousa, P. C., Vega, E. J., Sousa, R. G., Montanero, J. M., & Alves, M. A. (2017). Measurement of relaxation times in extensional flow of weakly viscoelastic polymer solutions. *Rheologica Acta*, *56*(1), 11–20. https://doi.org/10.1007/s00397-016-0980-1

Tao, J., & Shivkumar, S. (2007). Molecular weight dependent structural regimes during the electrospinning of PVA. *Materials Letters*, *61*(11–12), 2325–2328. https://doi.org/10.1016/J.MATLET.2006.09.004

Tirel, C., Renoult, M.-C. C., Dumouchel, C., Lisiecki, D., Crumeyrolle, O., & Mutabazi, I. (2017). Multi-scale analysis of a viscoelastic liquid jet. *Journal of Non-Newtonian Fluid Mechanics*, *245*, 1–10. https://doi.org/10.1016/j.jnnfm.2017.05.001

Tirtaatmadja, V., McKinley, H. G., & Cooper-White, J. J. (2006). Drop formation and breakup of low viscosity elastic fluids: Effects of molecular weight and concentration. *Physics of Fluids*, *18*(4). https://doi.org/10.1063/1.2190469

Wan, F., Larsen, F. H., Bordallo, H. N., Foged, C., Rantanen, J., & Yang, M. (2018). Insight into Nanoscale Network of Spray-Dried Polymeric Particles: Role of Polymer Molecular Conformation. *ACS Applied Materials & Interfaces*, *10*(43), 36686–36692. https://doi.org/10.1021/acsami.8b12475

FIGURE CAPTIONS

Figure 1. a) Zero-shear rate viscosity as a function of a dimensionless concentration parameter (from Modesto-López *et al*. (2019)), b) Schematics of the cross-section view of a FB atomizer, c) Shear viscosity as a function of shear rate for PEO solutions atomized in this study.

Figure 2. Calibration curve of the Flow Blurring device for each gas pressure, P_G, employed in this work, where Q_ℓ is the measured solution flow rate, P_L is the liquid pressure, and $P_G^* = P_G - P_o$.

Figure 3. Frames from high-speed videos of two PEO solutions atomized with a FB device a) 100k 2 % wt right at the atomizer outlet, $z = 0\ cm$, and b) $z = 4\ cm$; and 600k 0.1 % wt c) at $z = 0\ cm$, and d) – f) $z = 4\ cm$. The red oval indicates droplets linked by a filament. The red arrows point out filaments stemming from droplets. The white dashed line indicates the atomizer's wall.

Figure 4. High-speed video frames of FB atomization of PEO 600 k 0.1 wt% (1.71 cP) recorded in the vicinity of the atomizer outlet. The images depict not the entire frame but only the lower half. The gray bar on the left side of some frames indicates the atomizer. Red ovals indicate the evolution of polymeric structures, and the white, dashed line highlights a polymer filament.

Figure 5. a) sequential images of the impact of two PEO droplets (100k, 1.5 wt%) and subsequent filament elongation (frames 1-14). The time between each frame is 1 μs. b) Dimensionless radius $R^* = R/R_0$ as a function of dimensionless time τ^*, where the inertio-capillary and elasto-capillary regimes are observed.

Figure 6. Particle size distribution of a PEO 100k 1.5 wt% solution atomized at $P_G = 300\ kPa$ and varying Q_ℓ.

Figure 7. Non-dimensional diameter d_1^* as a function of non-dimensional diameter d_2^*. The mean diameters of the two main lines, d_1 and d_2, were made non-dimensional by the FB device's orifice diameter, D, that is $d_1^* = d_1/D$ and $d_2^* = d_2/D$.

Figure 8. Dimensionless diameter $d^+ = d_2/D_o$ as a function of GLR

Figure 9. Discharge coefficient (C_D) as a function of GLR at varying P_G. The solid lines show a power law fitting.

Figure 10. a) Reynolds number and b) Deborah number as a function of GLR.

FIGURES

Figure 1

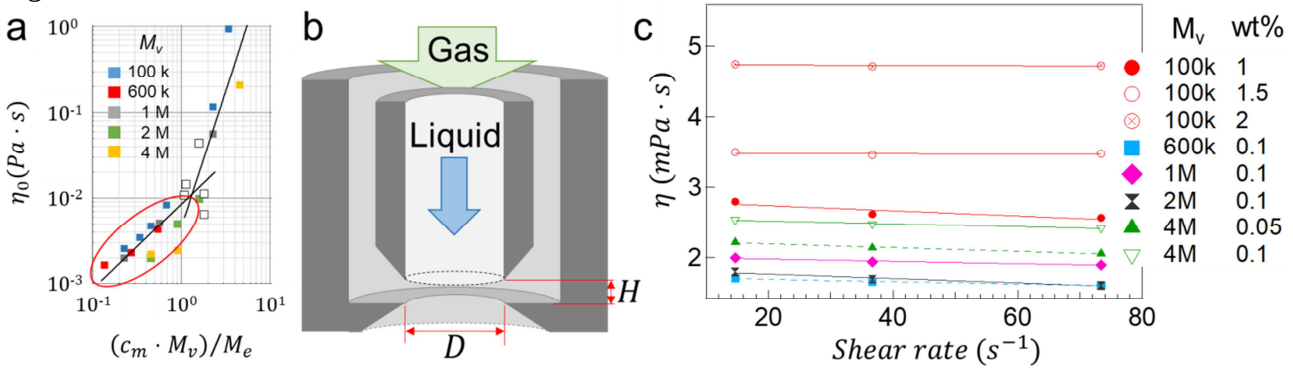

Figure 2

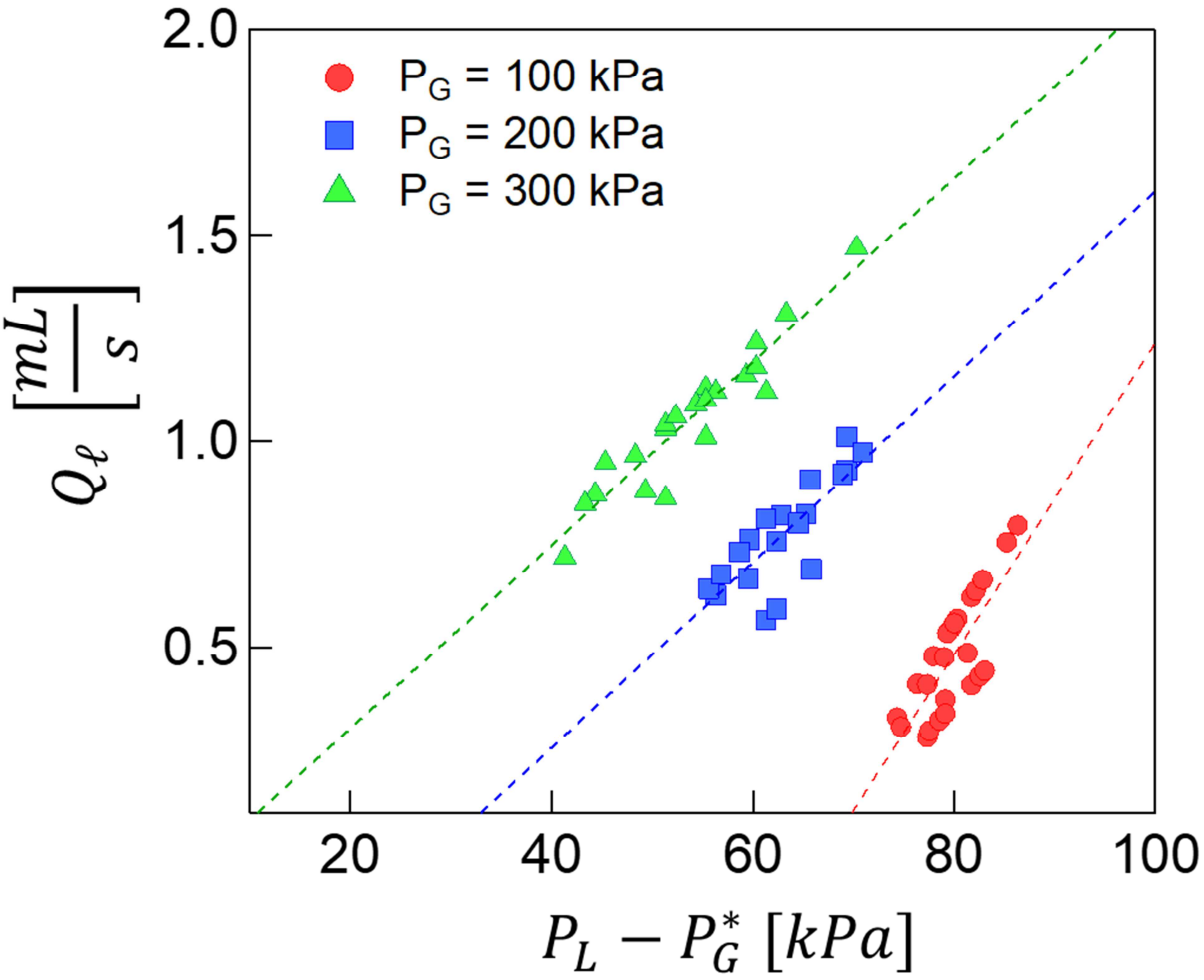

Figure 3

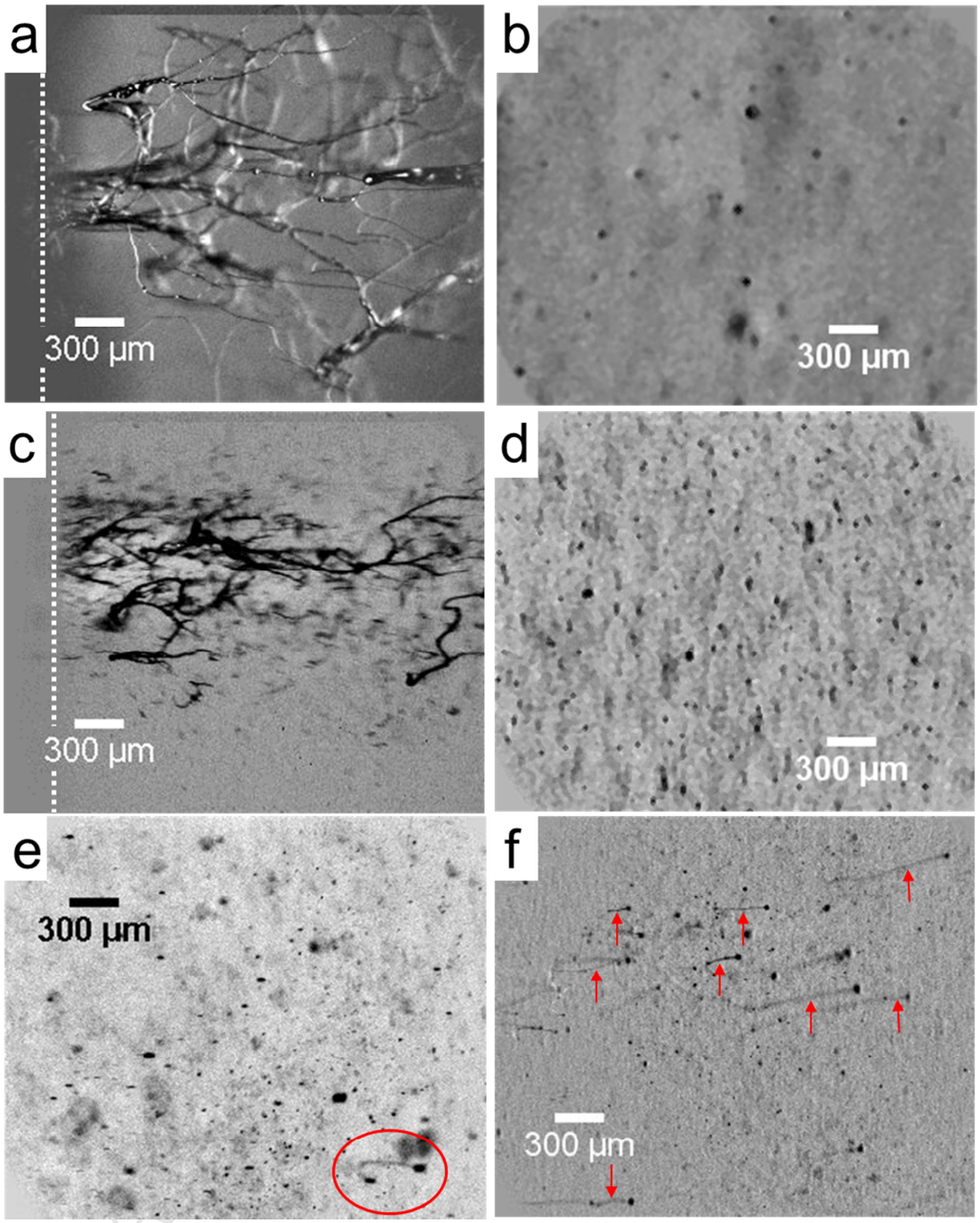

Figure 4

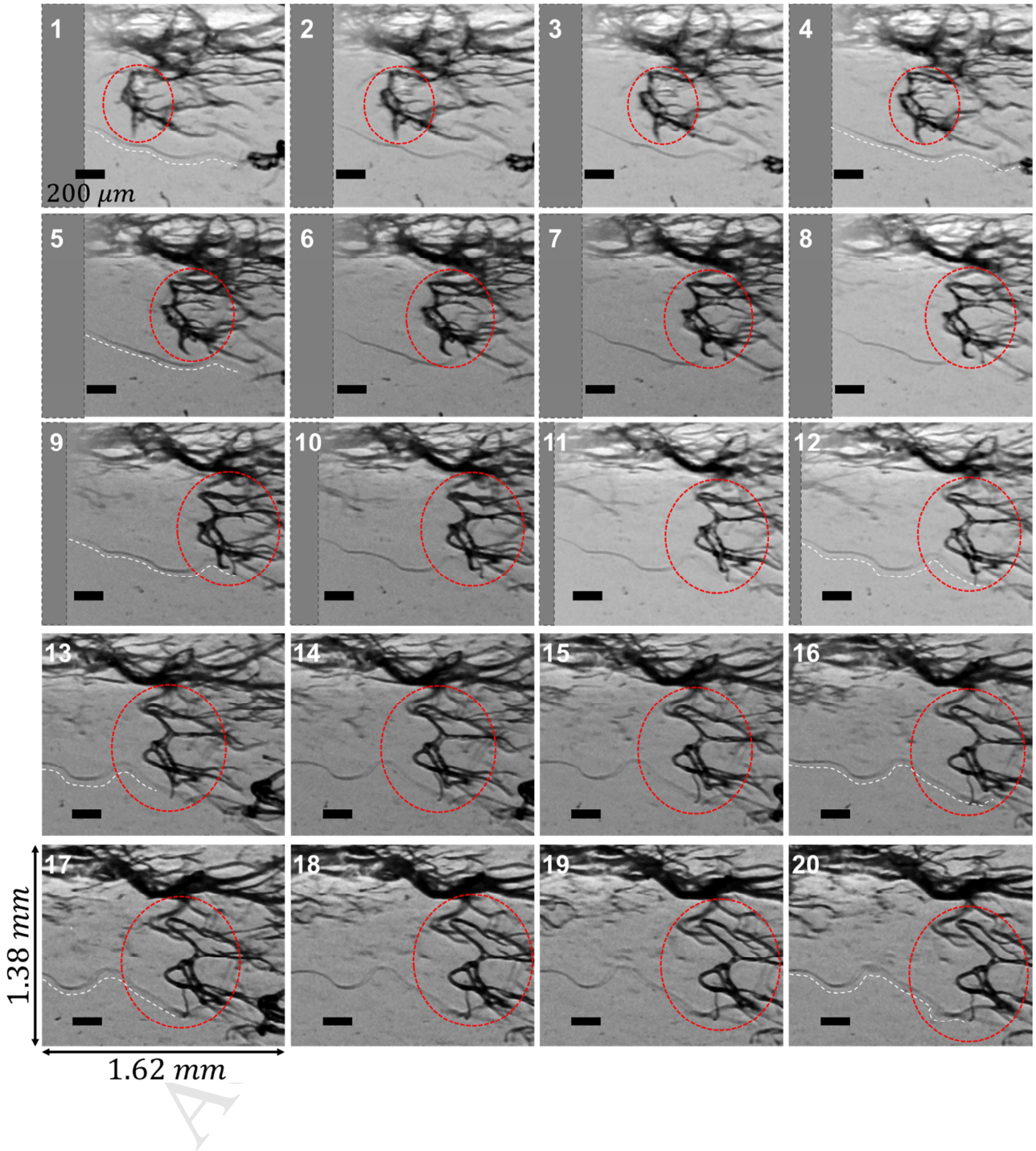

Figure 5

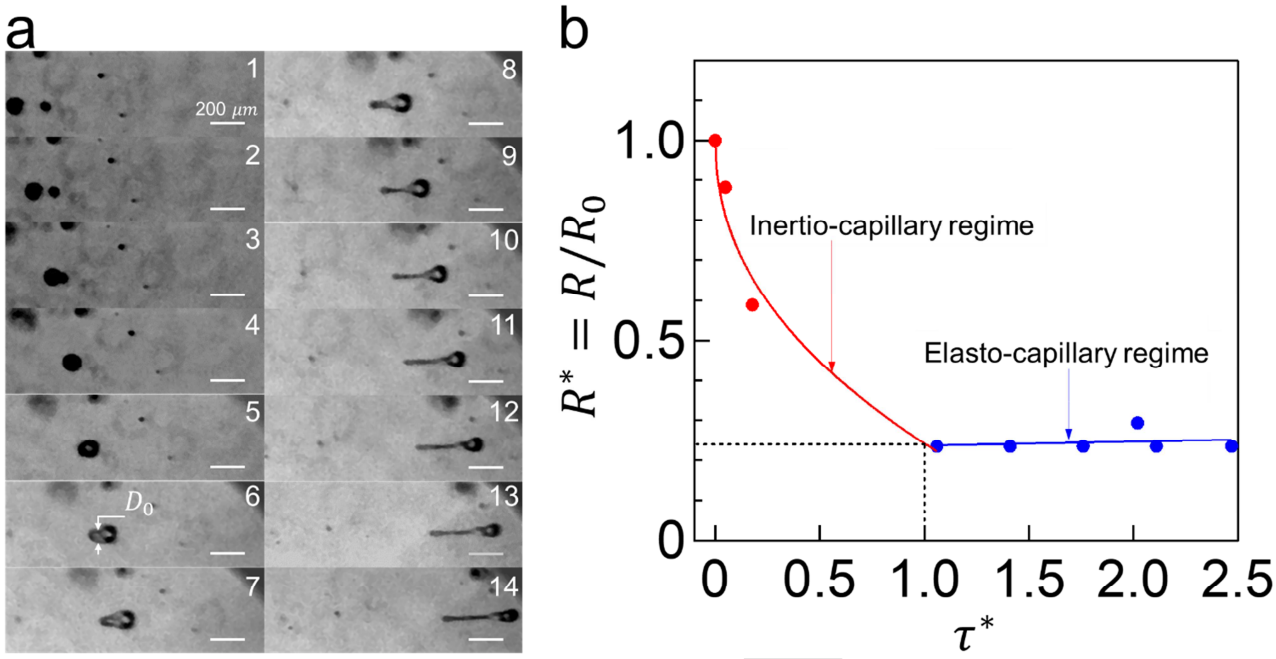

Figure 6

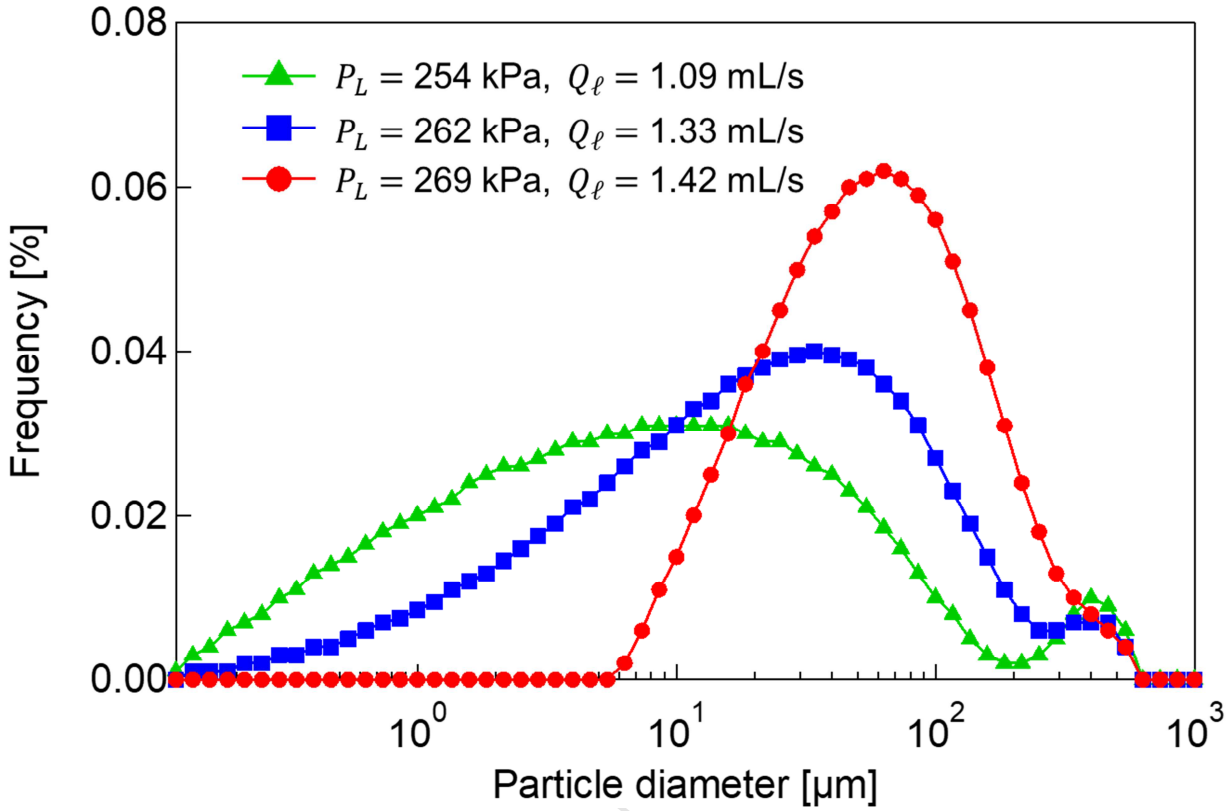

Figure 7

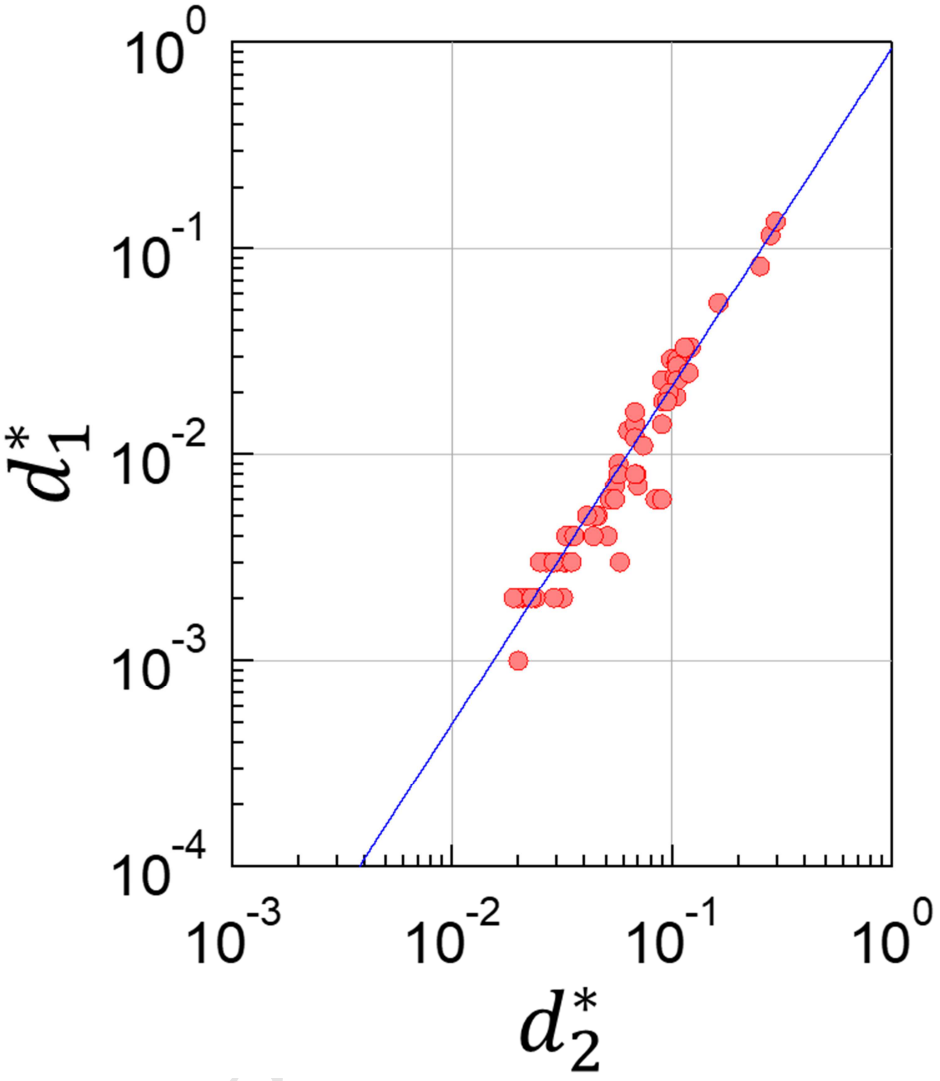

Figure 8

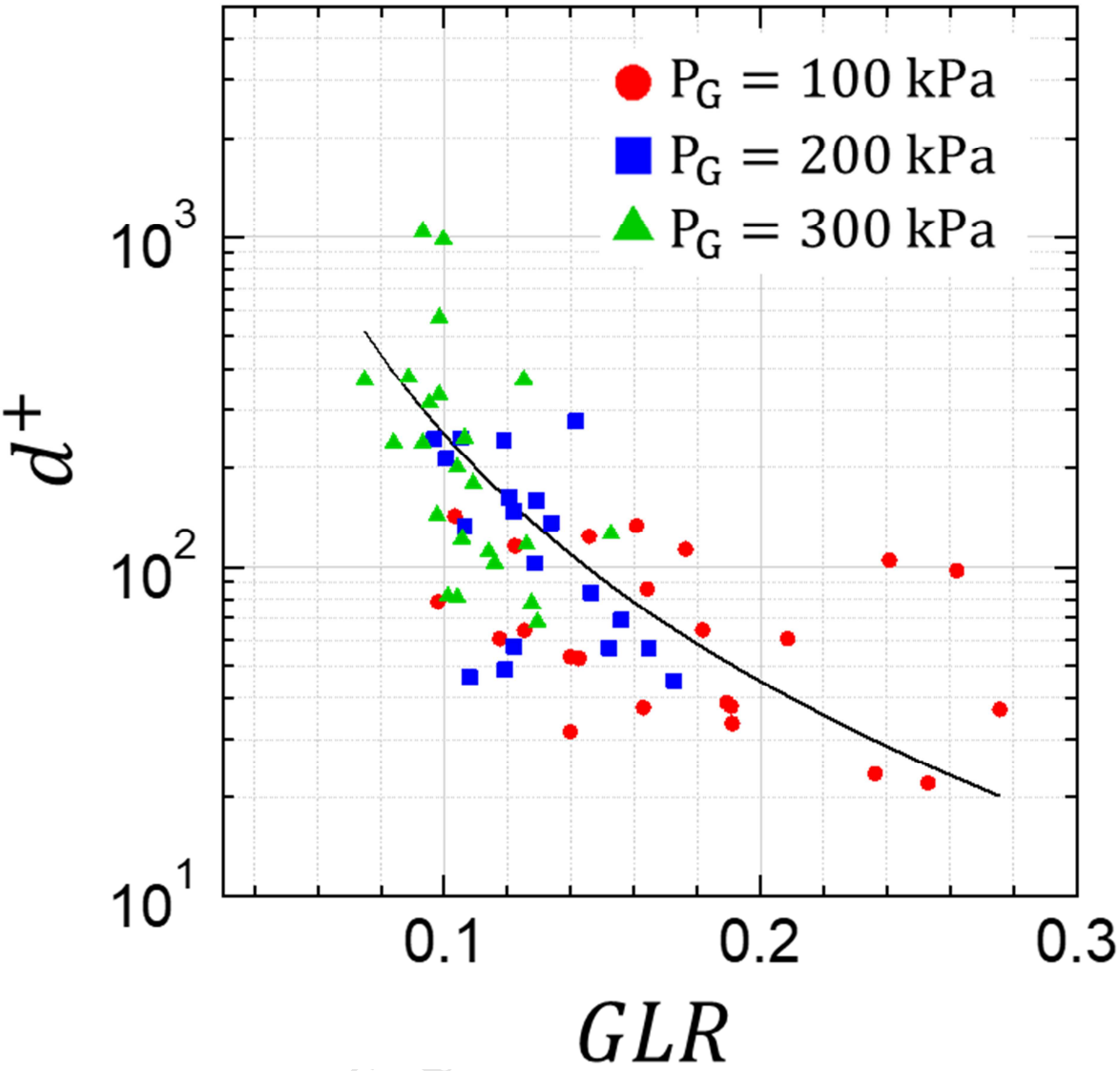

Figure 9

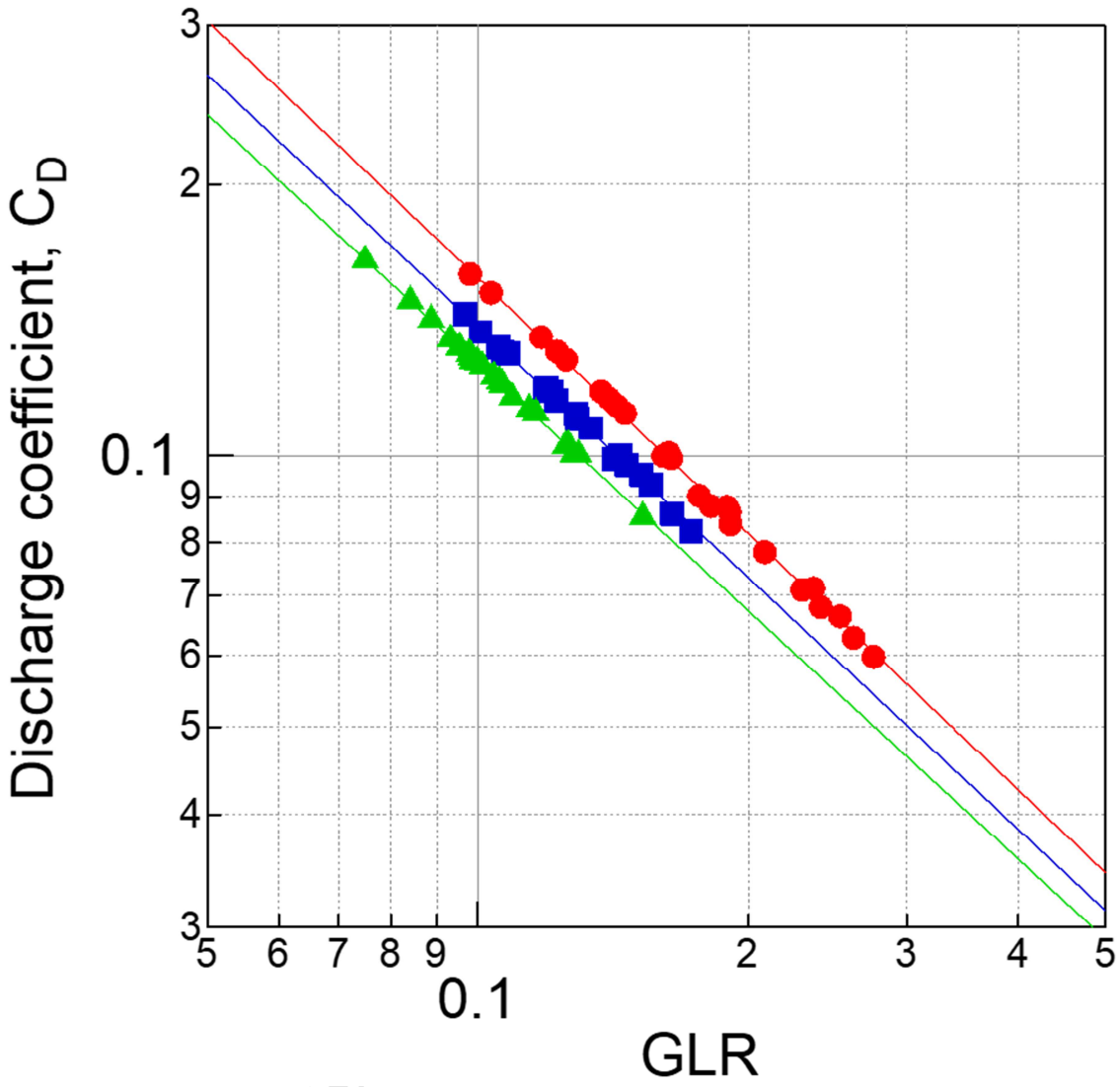

Figure 10

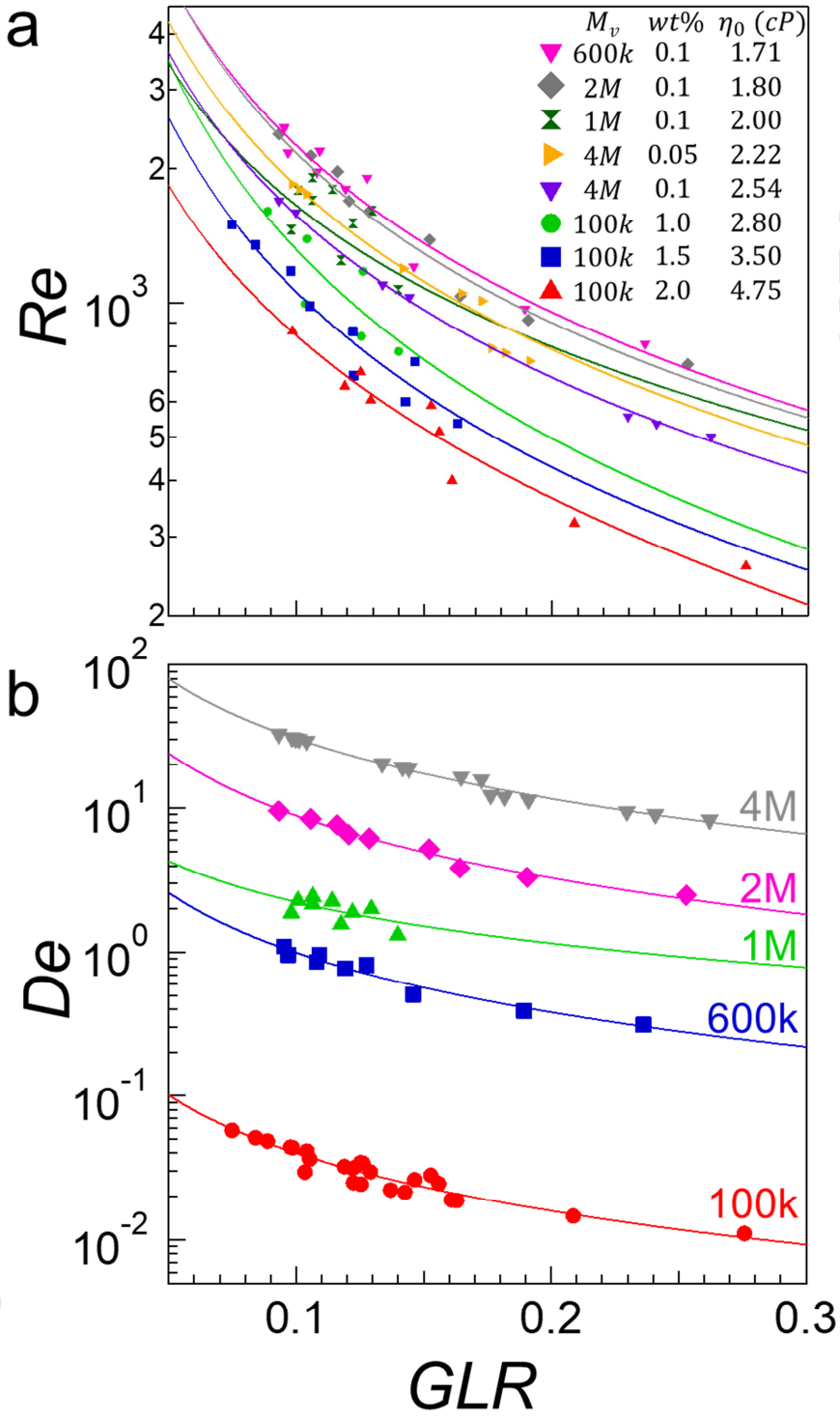
a
Re
M_v wt% η_0 (cP)
600k 0.1 1.71
2M 0.1 1.80
1M 0.1 2.00
4M 0.05 2.22
4M 0.1 2.54
100k 1.0 2.80
100k 1.5 3.50
100k 2.0 4.75
b
De
4M
2M
1M
600k
100k
GLR

Flow Blurring Atomization of Poly(ethylene oxide) Solutions below the Coil Overlap Concentration

Miguel Hermosín-Reyes, Alfonso M. Gañán-Calvo, Luis B. Modesto-López*

Highlights:

- Dilute PEO solutions show Newtonian-like shear viscosity
- Atomized droplets exhibit extensional viscosity in-flight
- Polymer filaments break into droplets in a time scale of the order of microseconds
- Mean droplet size of Flow Blurring-atomized solutions decreases with increasing GLR